



# Ni<sup>0</sup> NPs anchored on acid-activated montmorillonite (Ni<sup>0</sup>-Mont) as a highly efficient and reusable nanocatalyst for synthesis of biscoumarins and bisdimedones

Soleiman Rahmani<sup>1</sup> · Behzad Zeynizadeh<sup>1</sup>

Received: 18 May 2018 / Accepted: 18 November 2018  
© Springer Nature B.V. 2018

## Abstract

Ni<sup>0</sup> nanoparticles were immobilized on acid-activated montmorillonite (Ni<sup>0</sup>-Mont) by anchoring Ni(OAc)<sub>2</sub>·4H<sub>2</sub>O on modified micro/mesoporous montmorillonite followed by reduction with ethylene glycol. The prepared clay composite system was then characterized using Fourier-transform infrared (FT-IR) spectroscopy, scanning electron microscopy (SEM), energy-dispersive X-ray (EDX) spectroscopy, X-ray diffraction (XRD) analysis, and Brunauer–Emmett–Teller (BET) analysis. SEM analysis revealed perfect dispersion of metallic nickel nanoparticles with size distribution of 6–41 nm on the clay matrix. Micro/mesoporous montmorillonite was prepared by activation of Na<sup>+</sup>-montmorillonite with HCl (4 M) under controlled conditions. The catalytic activity of the prepared Ni<sup>0</sup>-Mont clay was studied in one-pot microwave-assisted synthesis of biscoumarins and bisdimedones via Knoevenagel reaction of aromatic aldehydes with 4-hydroxycoumarin or dimedone in solvent-free conditions. All reactions were carried out at room temperature within 5–15 min (for biscoumarins) and 5–20 min (for bisdimedones) to afford the products in high to excellent yield. The reusability of the Ni<sup>0</sup>-Mont catalyst was also investigated in seven consecutive cycles, without significant loss of catalytic activity.

**Keywords** Biscoumarins · Bisdimedones · Knoevenagel · Microwave · Montmorillonite K10 · Ni<sup>0</sup>-Mont

## Introduction

Transition-metal nanoparticles (NPs) are currently attracting a great deal of attention due to their prominent properties such as antifungal and antibacterial activities, being widely used in optical, electrical, magnetic, and sensor devices as well as drug

✉ Behzad Zeynizadeh  
bzeynizadeh@gmail.com

<sup>1</sup> Faculty of Chemistry, Urmia University, Urmia 5756151818, Iran

delivery systems [1–5]. In addition, their huge surface area and nanosize dimension accompanied by electronic effects of the metal species make them attractive catalysts for promotion of numerous organic reactions [6]. In this context, because of their unique chemical characteristics, air stability, high catalytic activity, easy preparation, and perfect recyclability, application of nickel nanoparticles has attracted attention from chemists in many fields [7–9]. Review of the literature shows that applications of nickel nanoparticles in Suzuki coupling [10–12], reductive amination of aldehydes [13], Mizoroki–Heck reaction [14, 15], oxidative Heck reaction [16], Hantzsch 1,4-dihydropyridine synthesis [17], synthesis of 2-arylbenzimidazoles, 2-arylbenzothiazoles, and azomethines [18], and pyran derivatives [19] has also been documented.

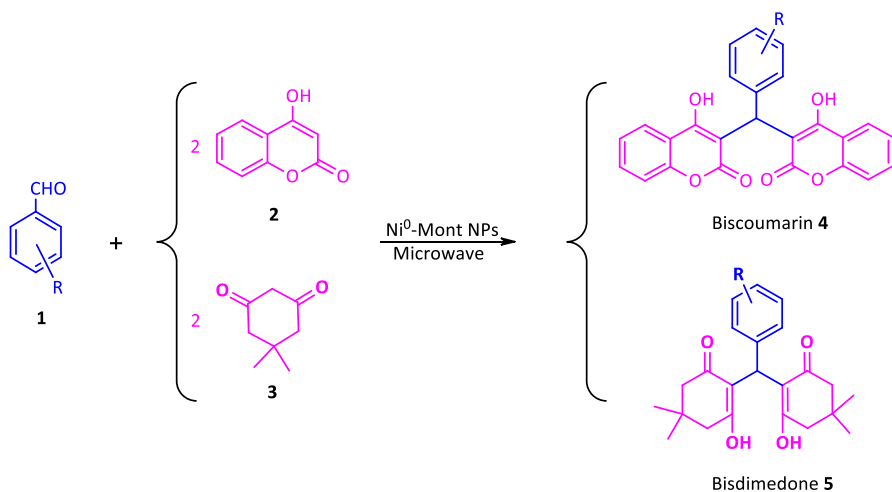
In spite of the great convenience of transition-metal nanoparticles for promotion of chemical reactions, they have a strong tendency for agglomeration, which diminishes their active surface area [20, 21]. Incorporation of numerous stabilizers or solid supports to immobilize transition-metal nanoparticles plays an important role in preventing agglomeration and to control their shape, morphology, and size distribution. In this field, alkylammonium salts [22], organic ligands [23], carbohydrates [24], filamentous carbon [25], and surfactants [26, 27] are the most commonly used stabilizers. Moreover, mesoporous materials including SBA-12 [28], resins [29], nanocrystalline MgO [30], and clay minerals [31–36] can also be applied as media for supporting transition-metal nanoparticles.

Clays are a class of materials that are widely available in Nature, generally being categorized into two groups, viz. cationic (clay minerals) and anionic clays (known as layered double hydroxides, LDHs). Cationic clays are constituted from colloidal layered hydrous aluminosilicates including  $\text{Si}(\text{O},\text{OH})_4$  tetrahedral and  $\text{M}(\text{O},\text{OH})_6$  octahedral ( $\text{M} = \text{Al}^{3+}$ ,  $\text{Mg}^{2+}$ ,  $\text{Fe}^{3+}$  or  $\text{Fe}^{2+}$ ). In addition, they can be further classified on the basis of the layer type and charge as well as the appearance of both Brønsted and Lewis acid properties produced by OH groups and  $\text{Al}^{3+}$  ions, respectively, in tetrahedral sheets. Various combinations of tetrahedral and octahedral layers result in clays with different properties [33]. Clay minerals of the smectite group such as montmorillonite K10, hectorite, saponite, and laponite are suitable solid supports for metal nanoparticles, which can be immobilized into the interlamellar spaces. Montmorillonite K10, in both its natural and modified forms, possesses both Brønsted and Lewis acid characteristics, which enables it to function as a perfect solid support or promoter. In addition, treatment of montmorillonite with acids or organic materials can dramatically improve properties such as its surface area and porosity [34, 35].

Biscoumarins (dicoumarols) are widely used precursors in synthesis of acridin-ediones (as laser dyes) and heterocyclic compounds [37]. Review of the literature shows that many coumarin and biscoumarin (dicoumarol) compounds exhibit a broad spectrum of biological activities, including antiinflammatory, antibacterial, anticancer, antiviral, anti-human immunodeficiency virus (HIV), and antiproliferative properties [38–44]. It has also been reported that some dicoumarol-based inhibitors exhibit activity against Gram-positive bacteria [45, 46]. Accordingly,

synthesis of dicoumarols is a subject of high interest. Generally, dicoumarols are prepared by condensation of 4-hydroxycoumarin with aromatic aldehydes in various solvents. Molecular iodine [47], piperidine [48], 1,8-diazabicyclo[5.4.0]undec-7-ene (DBU) [49], *n*-dodecylbenzene sulfonic acid (DBSA) [50], sodium dodecyl sulfate (SDS) [51], Zn(proline)<sub>2</sub> [52], tetra-*n*-butylammonium bromide (TBAB) [53], ionic liquids [54], and nanosilica chloride [55] are some of the catalysts/reagents reported for promotion of the title reaction. As well as synthesis of biscoumarin compounds, preparation of bisdimedones as raw materials to afford xanthan products has also attracted attention from research groups in laboratory and industrial settings [56, 57]. Due to their antibacterial, antiviral, antiinflammatory, and analgesic activities, xanthene derivatives are very important compounds [58], being variably used as dyes [59] in laser technology [60] and as fluorescent probes for measuring pH values of living chondrocytes [61]. As well, some xanthenediones are important building blocks in natural products [62]. Although the mentioned methods have their own merits, most of them suffer from disadvantages such as prolonged reaction time, tedious workup procedure, unsatisfactory yield, high temperature, or use of expensive and unrecoverable catalysts. Thus, development of new and more efficient catalytic systems for use under green reaction conditions is still required.

In line with the outlined strategies, we introduce herein a highly efficient protocol for one-pot microwave-assisted synthesis of biscoumarins and bisdimedones by Knoevenagel condensation reaction of 4-hydroxycoumarin or dimedone with aromatic aldehydes in presence of Ni<sup>0</sup> NPs anchored on acid-activated montmorillonite (Ni<sup>0</sup>-Mont) as a green, efficient, and easily reusable clay-based catalyst (Scheme 1).



**Scheme 1** Synthesis of biscoumarin 4 and bisdimedone 5 catalyzed by Ni<sup>0</sup>-Mont NPs system

## Experimental

### Materials and methods

All chemicals were purchased from chemical companies with best quality and were used without further purification.  $^1\text{H}$  and  $^{13}\text{C}$  nuclear magnetic resonance (NMR) and FT-IR spectra were recorded on 300 MHz Bruker Avance and Thermo Nicolet Nexus 670 spectrometers. Particle size and morphology were determined by scanning electron microscopy (SEM) and energy dispersive X-ray (EDX) spectroscopy. Melting points were recorded on Electrothermal 9100 melting point apparatus and are uncorrected. All products are known and were characterized by comparison of their physical and spectral data with reported values. Yields refer to isolated pure products. Thin-layer chromatography (TLC) over silica gel 60 F254 aluminum sheet was used to monitor the reactions. Microwave irradiation was carried out in a domestic microwave oven (LG MS-2344B, 1250 W). Montmorillonite K10 was purchased from Sigma-Aldrich company (art. no. 69866,  $\text{pH} \sim 3\text{--}4$ , surface area  $250 \text{ m}^2/\text{g}$ ).

### Preparation of homoionic $\text{Na}^+$ -exchanged montmorillonite ( $\text{Na}^+$ -Mont)

In a beaker (250 mL) containing distilled water (200 mL), montmorillonite K10 (5 g) was added and the mixture was stirred vigorously at room temperature for 20 h. The mixture was then allowed to settle, and the aqueous phase was decanted. To the obtained solid residue, aqueous solution of NaCl (2 M, 200 mL) was added and stirring was continued for 2 h at room temperature. The aqueous phase was decanted, and the solid residue was again charged with aqueous solution of NaCl (2 M, 200 mL). After stirring for 2 h at room temperature, the aqueous phase was decanted. The procedure was repeated an additional two times. Finally, the solid residue was washed frequently with distilled water until the conductivity of the liquid filtrate reached the conductivity of distilled water. The solid residue was dried at  $50 \text{ }^\circ\text{C}$  under air atmosphere to afford homoionic  $\text{Na}^+$ -exchanged montmorillonite ( $\text{Na}^+$ -Mont) [32].

### Preparation of acid-activated montmorillonite ( $\text{H}^+$ -Mont)

To a round-bottomed flask (250 mL) containing aqueous solution of HCl (4 M, 100 mL),  $\text{Na}^+$ -Mont (5 g) was added. The mixture was stirred under reflux conditions for 2 h. After cooling, the aqueous phase was decanted, and the residue was washed frequently with distilled water. When the liquid filtrate was free of  $\text{Cl}^-$  (tested with  $\text{AgNO}_3$ ), the solid material on filter paper was collected and dried at  $50 \text{ }^\circ\text{C}$  to afford acid-activated montmorillonite ( $\text{H}^+$ -Mont).

## Preparation of Ni<sup>0</sup> NPs immobilized on acid-activated montmorillonite [Ni<sup>0</sup>-Mont]

In a beaker (100 mL) containing aqueous solution of Ni(OAc)<sub>2</sub>·4H<sub>2</sub>O (0.05 M, 10 mL), acid-activated montmorillonite (0.5 g) was added portionwise, and the resulting mixture was stirred vigorously at room temperature for 6 h. The aqueous phase was then evaporated under reduced pressure. The dried Mont-Ni(OAc)<sub>2</sub> was dispersed in ethylene glycol (50 mL) within a double-necked round-bottomed flask. The mixture was stirred under reflux conditions for 6 h (N<sub>2</sub> atmosphere). Ethylene glycol was then removed by decantation, followed by washing the solid residue with MeOH to remove remaining ethylene glycol. The solid material was then dried at 40 °C for 12 h (N<sub>2</sub> flow), giving Ni<sup>0</sup> NPs anchored on acid-activated montmorillonite (Ni<sup>0</sup>-Mont).

## General procedure for synthesis of biscoumarins/bisdimedones using Ni<sup>0</sup>-Mont NPs

In a watch glass (diameter 5 cm), a mixture of 4-hydroxycoumarin/dimedone (2 mmol), aromatic aldehyde (1 mmol), Ni<sup>0</sup>-Mont (0.02 g), and 3–4 drops absolute ethanol was well mixed, and the resulting mushy mixture was irradiated in a domestic microwave oven (850 W) for an appropriate time as mentioned in Tables 4 and 5. After reaction completion (monitored by TLC), the mixture was cooled to room temperature. Ethyl acetate (5 mL) was then added, and the mixture was stirred for 5 min. The catalyst was removed from the reaction mixture using a filter paper. The filtrate was evaporated, and the solid material was recrystallized from hot ethanol to afford pure biscoumarin/bisdimedone materials (yield 75–95 %).

## Cation-exchange capacity (CEC) of the clay mineral

The cation-exchange capacity (CEC) of the clay mineral was determined according to the reported procedure [21]. To do this, clay mineral (such as Mont K10) (0.5 g) was dispersed in standard alcoholic solution of CaCl<sub>2</sub> (10 mL, 0.05 M), and the prepared mixture was stirred at room temperature for 24 h. The suspension was filtered, washed with EtOH (20 mL), and dried at room temperature for 12 h. The Ca<sup>2+</sup>-exchanged clay mineral was then transferred to a volumetric flask (250 mL). The volume in the flask was increased by adding distilled water to reach the standard limit (250 mL). The amount of Ca<sup>2+</sup> was titrated with standard solution of ethylenediaminetetraacetic acid (EDTA). The difference between the Ca<sup>2+</sup> concentration before and after cation exchange affords the CEC (meq/g) value of the clay mineral.

## Spectral data for prepared biscoumarin and bisdimedone materials

**3,3'-(Phenylmethylene)-bis(4-hydroxy-2H-chromen-2-one) (4a)** FT-IR (KBr,  $\nu$  cm<sup>-1</sup>): 3400, 3067, 2737, 1659, 1609, 1564, 1336, 1089, 755; <sup>1</sup>H NMR (300 MHz, CDCl<sub>3</sub>):  $\delta$  (ppm) 6.11 (s, 1H, CH), 7.25–8.07 (m, 13H, ArH), 11.32 (s, 1H, OH),

11.55 (s, 1H, OH);  $^{13}\text{C}$  NMR (75 MHz,  $\text{CDCl}_3$ ):  $\delta$  (ppm) 36.16, 103.88, 105.62, 116.42, 116.65, 124.39, 124.91, 126.89, 128.77, 132.88, 135.17, 152.27, 164.60, 165.02.

**3,3'-(2,4-Dichlorophenylmethylene)-bis(4-hydroxy-2H-chromen-2-one) (4b)** FT-IR (KBr,  $\nu$   $\text{cm}^{-1}$ ): 3068, 2719, 2594, 1649, 1565, 1497, 1097, 759;  $^1\text{H}$  NMR (300 MHz,  $\text{CDCl}_3$ ):  $\delta$  (ppm) 6.12 (s, 1H, CH), 7.24–8.02 (m, 11H, ArH), 11.67 (s, 2H, OH);  $^{13}\text{C}$  NMR (75 MHz,  $\text{CDCl}_3$ ):  $\delta$  (ppm) 35.46, 116.51, 124.48, 124.87, 126.9, 130.33, 132.92, 134.1, 152, 164.22, 166.8.

**3,3'-(4-Chlorophenylmethylene)-bis(4-hydroxy-2H-chromen-2-one) (4c)** FT-IR (KBr,  $\nu$   $\text{cm}^{-1}$ ): 3428, 3073, 2730, 1664, 1614, 1565, 1494, 1344, 1094, 770;  $^1\text{H}$  NMR (300 MHz,  $\text{CDCl}_3$ ):  $\delta$  (ppm) 6.04 (s, 1H, CH), 7.15–8.06 (m, 12H, ArH), 11.32 (s, 1H, OH), 11.55 (s, 1H, OH);  $^{13}\text{C}$  NMR (75 MHz,  $\text{CDCl}_3$ ):  $\delta$  (ppm) 35.7, 103.69, 105.24, 116.34, 124.41, 125.01, 127.97, 128.77, 132.77, 133.04, 133.83, 152.26, 164.53, 166.02.

**3,3'-(2-Chlorophenylmethylene)-bis(4-hydroxy-2H-chromen-2-one) (4d)** FT-IR (KBr,  $\nu$   $\text{cm}^{-1}$ ): 3069, 2720, 1649, 1556, 1498, 1444, 1340, 1097, 760;  $^1\text{H}$  NMR (300 MHz,  $\text{CDCl}_3$ ):  $\delta$  (ppm) 6.16 (s, 1H, CH), 7.27–8.04 (m, 12H, ArH), 10.93 (s, 1H, OH), 11.64 (s, 1H, OH);  $^{13}\text{C}$  NMR (75 MHz,  $\text{CDCl}_3$ ):  $\delta$  (ppm) 35.72, 116.59, 124.42, 124.87, 126.76, 128.59, 129.24, 130.81, 132.83, 133.49, 162.33.

**3,3'-(4-Bromophenylmethylene)-bis(4-hydroxy-2H-chromen-2-one) (4e)** FT-IR (KBr,  $\nu$   $\text{cm}^{-1}$ ): 3428, 3068, 2930, 1663, 1612, 1563, 1490, 1445, 1342, 1315, 1200, 1096, 1022, 767;  $^1\text{H}$  NMR (300 MHz,  $\text{CDCl}_3$ ):  $\delta$  (ppm) 6.02 (s, 1H, CH), 7.09–8.06 (m, 12H, ArH), 11.32 (s, 1H, OH), 11.54 (s, 1H, OH);  $^{13}\text{C}$  NMR (75 MHz,  $\text{CDCl}_3$ ):  $\delta$  (ppm) 35.86, 103.64, 105.18, 116.36, 116.66, 120.87, 124.4, 124.97, 128.3, 131.69, 134.4, 152.28, 162.34, 164.63, 166.02.

**3,3'-(4-Methoxyphenylmethylene)-bis(4-hydroxy-2H-chromen-2-one) (4f)** FT-IR (KBr,  $\nu$   $\text{cm}^{-1}$ ): 3064, 2944, 2842, 2727, 1666, 1612, 1562, 1507, 1447, 1343, 1309, 1094, 768;  $^1\text{H}$  NMR (300 MHz,  $\text{CDCl}_3$ ):  $\delta$  (ppm) 3.80 (s, 3H, OMe), 6.05 (s, 1H, CH), 6.84–8.05 (m, 12H, ArH), 11.34 (s, 1H, OH), 11.52 (s, 1H, OH);  $^{13}\text{C}$  NMR (75 MHz,  $\text{CDCl}_3$ ):  $\delta$  (ppm) 33.37, 110.93, 116.5, 116.7, 120.4, 123.5, 124.3, 124.7, 128.2, 128.4, 132.44, 152.13, 157.56, 163.7, 165.2.

**3,3'-(2-Methoxyphenylmethylene)-bis(4-hydroxy-2H-chromen-2-one) (4g)** FT-IR (KBr,  $\nu$   $\text{cm}^{-1}$ ): 3412, 3069, 2981, 2724, 1654, 1620, 1550, 1494, 1448, 1337, 1305, 1094, 758;  $^1\text{H}$  NMR (300 MHz,  $\text{CDCl}_3$ ):  $\delta$  (ppm) 3.5 (s, 3H, OMe), 6.09 (s, 1H, CH), 6.85–8.04 (m, 12H, ArH), 11.22 (bs, 2H, OH);  $^{13}\text{C}$  NMR (75 MHz,  $\text{CDCl}_3$ ):  $\delta$  (ppm) 35.48, 104.18, 105.74, 113.98, 116.62, 116.89, 124.36, 124.86, 126.90, 127.61, 132.83, 152.25, 152.47, 164.51, 165.69, 169.25.

**3,3'-(*p*-Tolylmethylene)-bis(4-hydroxy-2H-chromen-2-one) (4h)** FT-IR (KBr,  $\nu$  cm<sup>-1</sup>): 3100, 2992, 2919, 1665, 1614, 1563, 1502, 1440, 1094, 765; <sup>1</sup>H NMR (300 MHz, CDCl<sub>3</sub>):  $\delta$  (ppm) 2.34 (s, 3H, CH<sub>3</sub>), 6.07 (s, 1H, CH), 7.12–8.04 (m, 12H, ArH), 11.34 (s, 1H, OH), 11.48 (s, 1H, OH); <sup>13</sup>C NMR (75 MHz, CDCl<sub>3</sub>):  $\delta$  (ppm) 20.97, 35.87, 116.61, 116.93, 124.37, 124.84, 126.36, 129.33, 132.77, 136.46, 152.47, 162.34, 164.5, 165.67.

**3,3'-(4-Hydroxyphenylmethylene)-bis(4-hydroxy-2H-chromen-2-one) (4i)** FT-IR (KBr,  $\nu$  cm<sup>-1</sup>): 3361, 3072, 2731, 1660, 1614, 1565, 1509, 1443, 1096, 762; <sup>1</sup>H NMR (300 MHz, CDCl<sub>3</sub>):  $\delta$  (ppm) 6.02 (s, 1H, CH), 6.77–8.02 (m, 12H, ArH), 11.48 (bs, 2H, OH); <sup>13</sup>C NMR (75 MHz, CDCl<sub>3</sub>):  $\delta$  (ppm) 35.49, 104.16, 115.64, 116.61, 124.37, 126.78, 127.75, 152.41, 154.66, 162.32.

**3,3'-(4-Nitrophenylmethylene)-bis(4-hydroxy-2H-chromen-2-one) (4j)** FT-IR (KBr,  $\nu$  cm<sup>-1</sup>): 3427, 3075, 2935, 1652, 1562, 1343, 1095, 762; <sup>1</sup>H NMR (300 MHz, CDCl<sub>3</sub>):  $\delta$  (ppm) 6.14 (s, 1H, CH), 7.27–8.17 (m, 12H, ArH), 11.39 (s, 1H, OH), 11.58 (s, 1H, OH); <sup>13</sup>C NMR (75 MHz, CDCl<sub>3</sub>):  $\delta$  (ppm) 36.18, 103.22, 104.62, 116.26, 116.73, 121.76, 122.12, 124.5, 125.17, 129.59, 132.7, 133.33, 137.9, 148.75, 152.35, 162.34, 166.59, 166.9.

**3,3'-(2-Nitrophenyl)methylene)-bis(4-hydroxy-2H-chromen-2-one) (4k)** FT-IR (KBr,  $\nu$  cm<sup>-1</sup>): 3433, 3076, 2722, 1652, 1618, 1561, 1532, 1450, 1352, 1309, 1099, 761; <sup>1</sup>H NMR (300 MHz, CDCl<sub>3</sub>):  $\delta$  (ppm) 6.64 (s, 1H, CH), 7.27–8.01 (m, 12H, ArH), 11.55 (bs, 2H, OH); <sup>13</sup>C NMR (75 MHz, CDCl<sub>3</sub>):  $\delta$  (ppm) 33.86, 103.71, 116.66, 124.57, 125.03, 128.19, 129.49, 131.9, 133.2, 149.76.

**3,3'-(4-Pyridylmethylene)-bis(4-hydroxy-2H-chromen-2-one) (4l)** FT-IR (KBr,  $\nu$  cm<sup>-1</sup>): 3447, 3075, 2880, 1663, 1618, 1543, 1500, 1407, 1102, 757; <sup>1</sup>H NMR (300 MHz, DMSO-d<sub>6</sub>):  $\delta$  (ppm) 6.47 (s, 1H, CH), 7.21–8.68 (m, 12H, ArH and pyridyl-H). It is notable that, due deuterium exchange, hydrogen of two OH groups at region of  $\delta$  = 11.5 ppm was not observed. <sup>13</sup>C NMR (75 MHz, DMSO-d<sub>6</sub>):  $\delta$  (ppm) 38.26, 101.88, 116.20, 119.82, 123.65, 124.67, 125.67, 132.04, 141.35, 153.15, 164.53, 165.34, 168.59.

**2,2'-(Phenylmethylene)-bis(3-hydroxy-5,5-dimethylcyclohex-2-en-1-one) (5a)** FT-IR (KBr,  $\nu$  cm<sup>-1</sup>): 3434, 3038, 2852, 1719, 1593, 1447, 1378, 1405, 858, 746; <sup>1</sup>H NMR (300 MHz, CDCl<sub>3</sub>):  $\delta$  (ppm) 1.09 (s, 6H, CMe<sub>2</sub>), 1.23 (s, 6H, CMe<sub>2</sub>), 2.39 (bs, 8H, 2CH<sub>2</sub>), 5.56 (s, 1H, CH), 7.10–7.25 (m, 5H, Ar), 10.1 (br, 1H, OH), 11.91 (s, 1H, OH).

**2,2'-(2-Chlorophenyl)methylene)-bis(3-hydroxy-5,5-dimethylcyclohex-2-en-1-one) (5b)** FT-IR (KBr,  $\nu$  cm<sup>-1</sup>): 3339, 2954, 1718, 1596, 1458, 1387, 1288, 848, 753; <sup>1</sup>H NMR (300 MHz, CDCl<sub>3</sub>):  $\delta$  (ppm) 1.55 (s, 6H, CMe<sub>2</sub>), 1.073 (s, 6H, CMe<sub>2</sub>), 2.05–2.53 (m, 8H, 2CH<sub>2</sub>), 5.63 (s, 1H, CH), 7.12–7.39 (m, 4H, Ar), 11.86 (br, 1H, OH).

**2,2' -((4-Chlorophenyl)methylene)-bis(3-hydroxy-5,5-dimethylcyclohex-2-en-1-one) (5c)** FT-IR (KBr,  $\nu$   $\text{cm}^{-1}$ ): 3421, 3055, 2955, 1592, 1373, 1255, 836, 731;  $^1\text{H}$  NMR (300 MHz,  $\text{CDCl}_3$ ):  $\delta$  (ppm) 1.10 (s, 6H,  $\text{CMe}_2$ ), 1.21 (s, 6H,  $\text{CMe}_2$ ), 2.38 (bs, 8H,  $2\text{CH}_2$ ), 5.47 (s, 1H, CH), 7.02 (bs, 2H, Ar), 7.24 (bs, 2H, Ar), 11.76 (bs, 1H, OH), 11.86 (s, 1H, OH).

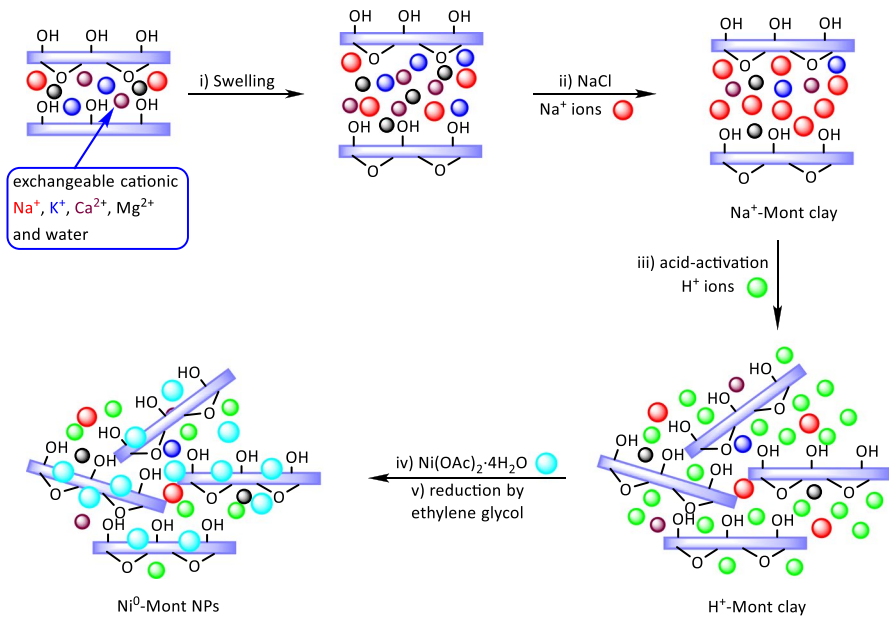
**2,2' -((3-Hydroxy-4-methoxyphenyl)methylene)-bis(3-hydroxy-5,5-dimethylcyclohex-2-en-1-one) (5d)** FT-IR (KBr,  $\nu$   $\text{cm}^{-1}$ ): 3425, 2951, 2643, 1721, 1594, 1520, 1373, 1270, 821, 758;  $^1\text{H}$  NMR (300 MHz,  $\text{CDCl}_3$ ):  $\delta$  (ppm) 1.31 (bs, 6H,  $\text{CMe}_2$ ), 1.40 (s, 6H,  $\text{CMe}_2$ ), 2.73–2.49 (m, 8H,  $2\text{CH}_2$ ), 3.84 (bs, 3H,  $\text{OCH}_3$ ), 5.47 (s, 1H, CH), 6.55–7.22 (m, 3H, Ar), 11.96 (bs, 1H, OH).

**2,2' -((4-nitrophenyl)methylene)-bis(3-hydroxy-5,5-dimethylcyclohex-2-enone) (5e)** FT-IR (KBr,  $\nu$   $\text{cm}^{-1}$ ): 3425, 2956, 2882, 1592, 1533, 1451, 1369, 1253, 887, 743;  $^1\text{H}$  NMR (300 MHz,  $\text{CDCl}_3$ ):  $\delta$  (ppm) 1.12 (s, 6H,  $\text{CMe}_2$ ), 1.27 (s, 6H,  $\text{CMe}_2$ ), 2.37–2.47 (m, 8H,  $2\text{CH}_2$ ), 5.54 (s, 1H, CH), 7.26 (m, 2H, Ar), 8.01 (s, 1H, Ar), 11.85 (s, 1H, OH).

## Results and Discussion

### Synthesis and characterization of $\text{Ni}^0$ NPs anchored on micro/mesoporous acid-activated montmorillonite ( $\text{Ni}^0$ -Mont)

Following the outlined strategies and due to the lack of information on montmorillonite-catalyzed synthesis of biscoumarins, we investigated the title transformation using  $\text{Ni}^0$  NPs immobilized on acid-activated montmorillonite K10 as a novel reusable clay-based catalyst. The study started with synthesis of the clay catalyst in a five-step procedure: (1) Preparation of swelled (hydrated) montmorillonite through vigorous stirring of commercially available montmorillonite K10 in distilled water. Similar to other clay minerals, montmorillonite K10 can absorb water between interlamellar spaces, moving the layers apart and swelling the clay, which expands the surface area of montmorillonite and exposes the cations of interlayers to contribute to the Brønsted and Lewis acid properties of the clay mineral [6]; (2) Preparation of homoionic  $\text{Na}^+$ -exchanged montmorillonite by adequate stirring of swollen montmorillonite in aqueous solution of NaCl. Through this and simple ion exchange, many cations of interlayers (of montmorillonite K10) are exchanged with  $\text{Na}^+$  ions. Diffusion of  $\text{Na}^+$  ions affords high capacity to the clay mineral for exchanging  $\text{Na}^+$  ions with various guest species (transition-metal ions/nanoparticles, complexes, and  $\text{H}^+$  ions) and their encapsulation in interlamellar spaces. Moreover, by altering the cations of the interlayers, the acidity (Brønsted and Lewis) of the clay mineral can be changed for different purposes; (3) Preparation of acid-activated montmorillonite by stirring homoionic  $\text{Na}^+$ -exchanged montmorillonite in aqueous solution of hydrochloric acid; (4) Preparation of immobilized  $\text{Ni}(\text{OAc})_2$  on acid-activated



**Scheme 2** Preparation of Ni<sup>0</sup>-Mont NPs system

montmorillonite by simply mixing and stirring of acid-activated montmorillonite in aqueous solution of nickel acetate; (5) Reduction of nickel acetate to nickel nanoparticles with ethylene glycol to obtain Ni<sup>0</sup>-Mont clay system (Scheme 2).

The concentration of exchangeable cations in a clay mineral is called its cation-exchange capacity (CEC), measured in milli-equivalent per 100 g of dried clay [36]. The measurement results for the CEC were 85 meq/g for Mont K10 and 110 meq/g for Na<sup>+</sup>-Mont, indicating that replacement of Na<sup>+</sup> ions of other cations in the interlayer spaces increased the cation-exchange capacity of the clay mineral.

After successful synthesis of the Ni<sup>0</sup>-Mont clay system, the size and morphology of Mont K10, acid-activated Mont (H<sup>+</sup>-Mont), and Ni<sup>0</sup>-Mont clays were studied using FT-IR, scanning electron microscopy (SEM), energy-dispersive X-ray (EDX) spectroscopy, and X-ray diffraction (XRD) analysis.

## FT-IR analysis

Fourier-transform infrared spectroscopy as a primarily tool was utilized for structural elucidation of montmorillonite K10 (Mont K10), acid-activated montmorillonite (H<sup>+</sup>-Mont), and Ni<sup>0</sup> immobilized on acid-activated montmorillonite (Ni<sup>0</sup>-Mont) (Fig. 1). The FT-IR spectrum of Mont K10 shows a wide absorption band at 3433 cm<sup>-1</sup> due to stretching vibration of hydroxyl groups bonded to Si, Al, and other metals that are present, a small absorption band at 1630 cm<sup>-1</sup> due to deformation vibration of hydroxyl groups, a strong absorption band at 1054 cm<sup>-1</sup> derived from stretching vibration of Si–O bonds in tetrahedral sites, a small absorption band at 795 cm<sup>-1</sup> due to the amorphous silica that is present, and bands at 522 and 464 cm<sup>-1</sup>

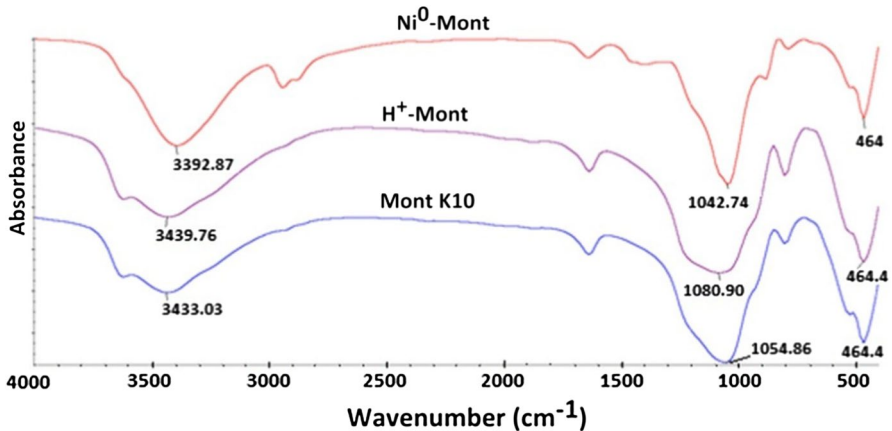
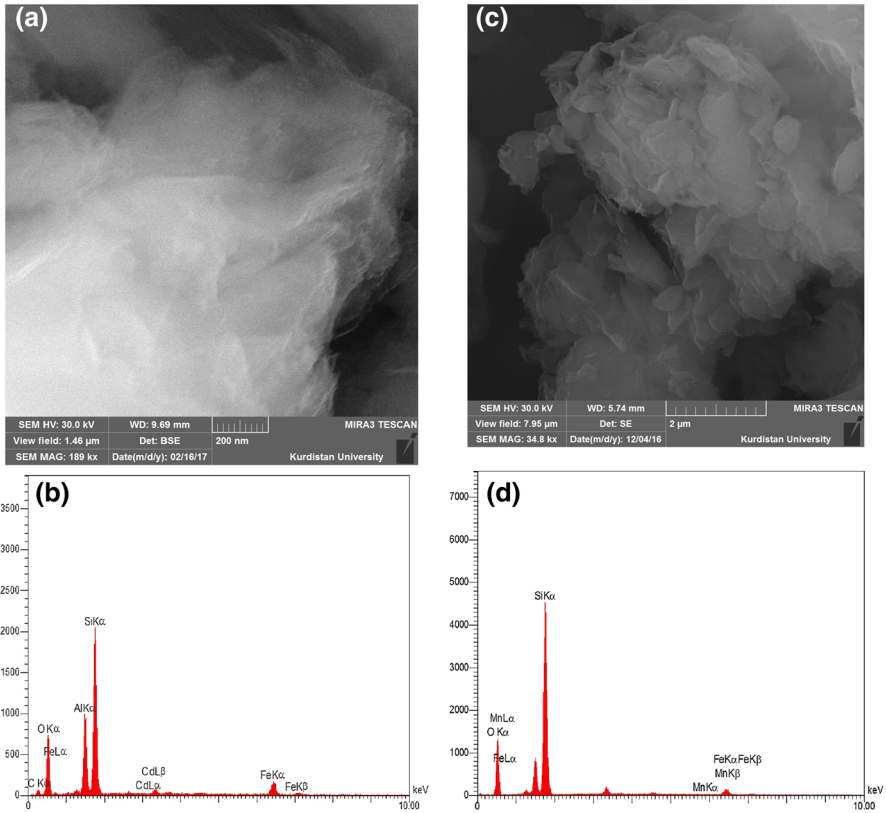


Fig. 1 FT-IR spectrum of Mont K10, H<sup>+</sup>-Mont, and Ni<sup>0</sup>-Mont clays

due to bending vibration of Si–O–Al and Si–O–Si bonds. In this context, the FT-IR spectrum of the H<sup>+</sup>-Mont and Ni<sup>0</sup>-Mont clay systems shows that, although they exhibited the same pattern as montmorillonite alone, the position of the wide stretching vibration of Si–O bonds of montmorillonite alone at 1054 cm<sup>-1</sup> was shifted to 1080 cm<sup>-1</sup> after acid activation, confirming successful ion exchange of the H<sup>+</sup>-Mont system. In the case of the Ni<sup>0</sup>-Mont system, the mentioned absorption peak shifted to 1042 cm<sup>-1</sup>, indicating dispersion of Ni<sup>0</sup> NPs on the surface of the montmorillonite clay. Also, the shape of the absorption band was modified, becoming narrower. In this context, the bands around 2948, 2865, and 1476 cm<sup>-1</sup> also confirm immobilization of nickel nanoparticles in the clay matrix through the conformational changes in metal-linked clay interactions [63–65]. It is notable that the structure of the clay matrix was unaffected when embedding nickel nanoparticles.

### SEM and EDX analysis

Further investigation towards elucidation of the clay composite systems was carried out by SEM and EDX spectroscopy to determine the elements presents. SEM images and EDX spectra of Mont K10 and H<sup>+</sup>-Mont clays are shown in Fig. 2. Comparing the SEM images (Fig. 2a, c) shows that, after acid activation, adjacent layers of Mont K10 were exfoliated to tiny segments. This phenomenon is attributed to elimination of many Al<sup>3+</sup> ions from octahedral sites in montmorillonite on reaction with HCl. It is notable that, due to the removal of Al<sup>3+</sup> ions from interlayers, numerous new pores were generated on the surface and in interlamellar spaces, increasing the surface area of the H<sup>+</sup>-Mont system compared with montmorillonite alone. In this context, the SEM analysis (Fig. 3) of the Ni<sup>0</sup>-Mont system exhibited anchored metallic nickel nanoparticles with spherical shape, well distributed on the surface of tiny segments or into interlamellar spaces, with particle size ranging from 6 to 41 nm. Accordingly, the illustrated EDX spectrum clearly demonstrates the presence of Ni content as well as other elements in the Ni<sup>0</sup>-Mont system.



**Fig. 2** a SEM image and b EDX spectrum of Mont K10, c SEM image and d EDX spectrum of H<sup>+</sup>-Mont system

## XRD analysis

In continuation, structural analysis of the clay composite systems was carried out by plotting the wide-angle XRD spectrum of the prepared samples (Fig. 4). Along with *hkl* and two-dimensional *hk* reflections, a number of sharp peaks corresponding to impurities (quartz, cristobalite, and feldspar) were observed in the diffractogram of Mont K10 (Fig. 4a). Accordingly, the XRD spectrum of the Na<sup>+</sup>-Mont system (Fig. 4b) clearly shows a significant increase in the intensity of the absorption peaks. This reveals that, through the simple ion-exchange process, Na<sup>+</sup> ions were successful incorporated into the interlamellar spaces, leading to a dramatic increase in the occupation of Na<sup>+</sup> ions [66, 67]. In spite of this, however, the intensity of the absorption peaks in the XRD pattern of the H<sup>+</sup>-Mont system (Fig. 4c) was clearly decreased. This phenomenon can be attributed to exfoliation and destruction of sheets in the Na<sup>+</sup>-Mont system by the HCl activation processing [68]. In the XRD pattern of the Ni<sup>0</sup>-Mont system (Fig. 4d), three characteristic peaks at  $2\theta = 44.5^\circ$ ,  $51.8^\circ$ , and  $76^\circ$ , marked with (111), (200), and (222) indices, respectively, reveal

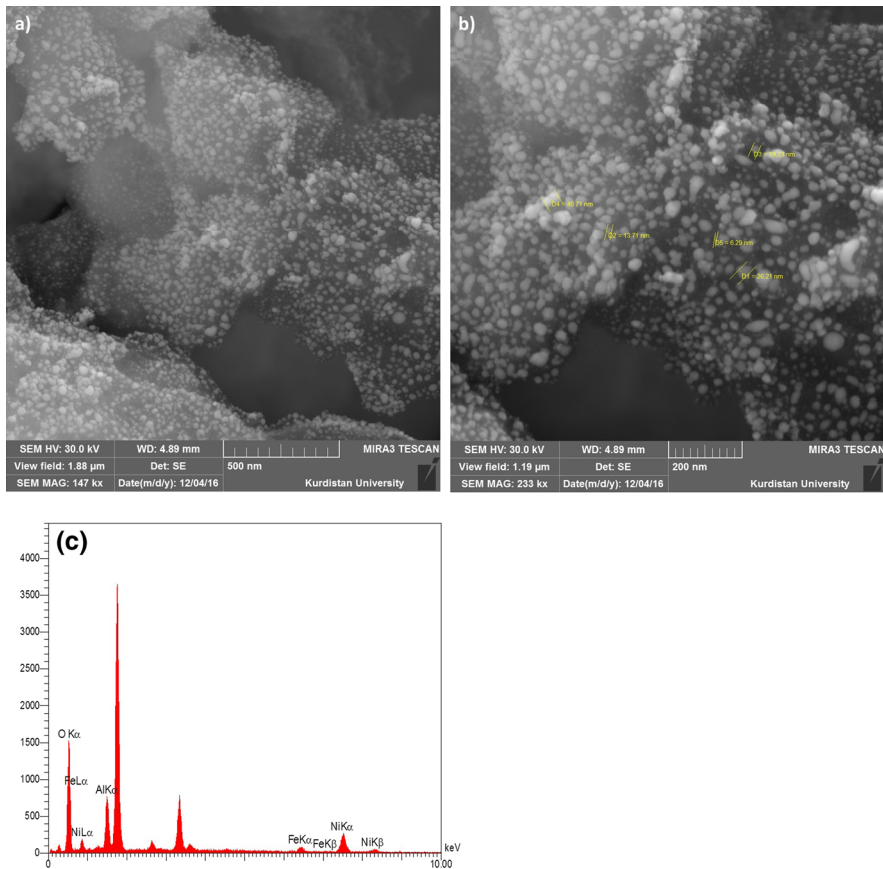


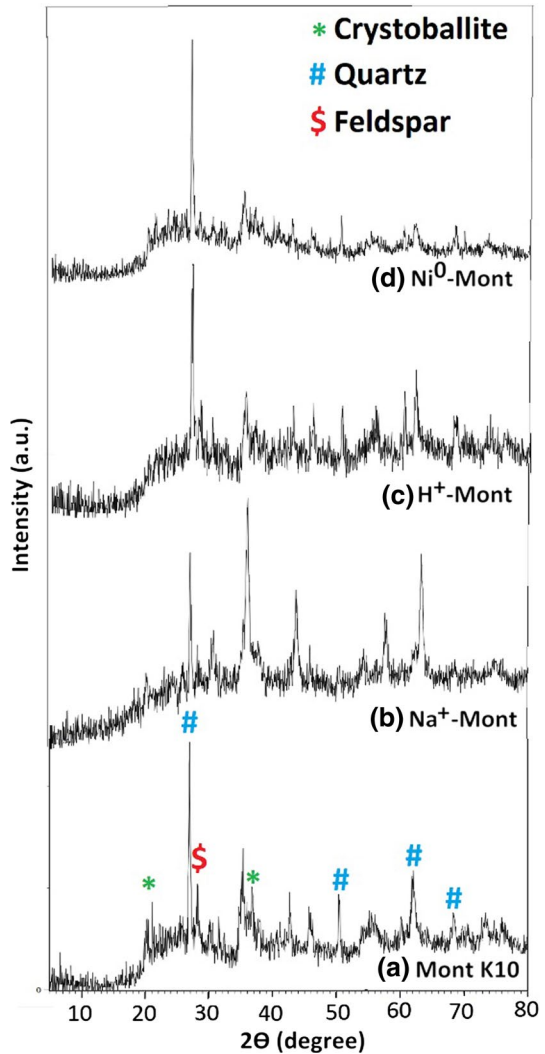
**Fig. 3** SEM and EDX spectrum of Ni<sup>0</sup>-Mont system

formation of pure Ni<sup>0</sup> NPs with face-centered cubic (fcc) structure on the surface of the clay matrix [69]. This means that no oxide or hydroxide of nickel was produced during the preparation of the Ni<sup>0</sup>-Mont system, confirming its phase purity [70].

### Ultraviolet–visible analysis

The immobilization of Ni<sup>0</sup> nanoparticles on acid-activated montmorillonite was also clarified using ultraviolet–visible (UV–Vis) spectroscopy. To do this, the UV–visible spectrum of Ni<sup>2+</sup> immobilized on acid-activated montmorillonite (before reduction) was plotted in the range of 630–780 nm (Fig. 5). As shown, the prepared Ni<sup>2+</sup>-Mont system exhibited a broad absorption band due to Ni<sup>2+</sup> species. Accordingly, when reduction of Ni<sup>2+</sup> species by polyethylene glycol was carried out to obtain Ni<sup>0</sup> NPs, the UV–Vis spectra did not show any absorption band. This analysis clearly demonstrates immobilization of Ni<sup>0</sup> NPs on the clay matrix [69, 70].

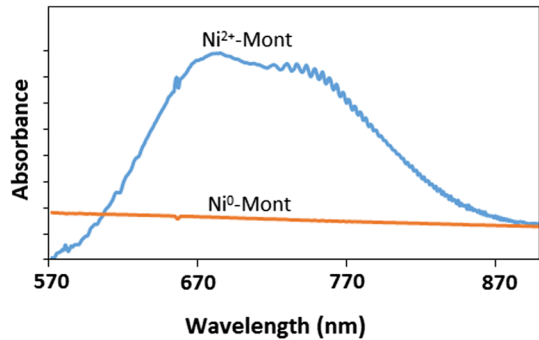
**Fig. 4** Wide-angle XRD patterns of **a** Mont K10, **b** Na<sup>+</sup>-Mont, **c** H<sup>+</sup>-Mont, and **d** Ni<sup>0</sup>-Mont systems



### BET analysis

To investigate the porosity and specific surface area of the clay composite systems, the N<sub>2</sub> adsorption–desorption isotherms of the Mont K10, H<sup>+</sup>-Mont, and Ni<sup>0</sup>-Mont systems are illustrated in Fig. 6. Analysis of this plot reveals that the pattern of isotherms is similar for all samples; according to the Brunauer–Deming–Deming–Teller (BDDT) classification, it is of type IV with H3 hysteresis loop. It is well known that this type of isotherm is characteristic of micro/mesoporous materials [71, 72]. As well, the parameters obtained for the examined samples (Table 1) show that the BET surface area and total pore volume of the H<sup>+</sup>-Mont system were increased compared with those of Mont K10

**Fig. 5** UV–Vis spectrum of  $\text{Ni}^{2+}$ -Mont and  $\text{Ni}^0$ -Mont clays in ethanol



alone. This can be attributed to acid activation of Mont K10, leading to exfoliation/destruction of adjacent sheets to tiny segments. Therefore, this action generated more new pores, affording the rise in pore volume and specific surface area [73, 74]. In contrast, anchoring  $\text{Ni}^0$  NPs on  $\text{H}^+$ -Mont clay reduced the BET surface area and total pore volume (due to blocking of pores in the  $\text{H}^+$ -Mont system by  $\text{Ni}^0$  NPs) accompanied with a significant increase in the average pore radius of particles. This increase could also arise due to rupture of some smaller pores towards bigger ones [21, 63, 75].

### Synthesis of biscoumarins and bisdimedones catalyzed by $\text{Ni}^0$ -Mont system

Next, the catalytic activity of the  $\text{Ni}^0$ -Mont clay system was studied in synthesis of biscoumarins via Knoevenagel condensation reaction of aromatic aldehydes with 4-hydroxycoumarin. To optimize the reaction conditions, the progress of the reaction of 4-hydroxycoumarin (2 mmol) and 4-chlorobenzaldehyde (1 mmol) in presence of  $\text{Ni}^0$ -Mont clay was investigated under different conditions. The

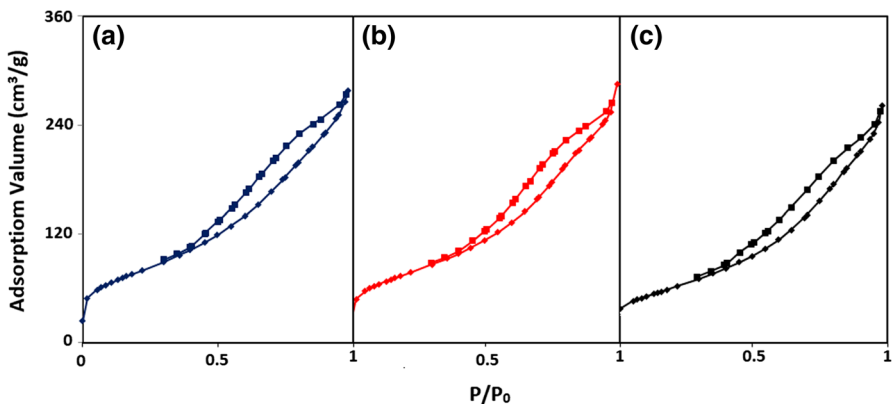


**Fig. 6**  $\text{N}_2$  adsorption–desorption isotherms of **a** Mont K10, **b**  $\text{H}^+$ -Mont, and **c**  $\text{Ni}^0$ -Mont systems

**Table 1** Surface properties of examined clay composite systems

Sample	$S_{\text{BET}}$ (m <sup>2</sup> g <sup>-1</sup> )	$V_{\text{m}}$ (cm <sup>3</sup> g <sup>-1</sup> )	Average pore diameter (nm)	$V_{\text{p}}$ (cm <sup>3</sup> g <sup>-1</sup> )	Total pore volume (cm <sup>3</sup> g <sup>-1</sup> )
Mont K10	250.11	51.835	6.427	0.4016	0.4298
H <sup>+</sup> -Mont	280.52	50.313	6.7483	0.419	0.5081
Ni <sup>0</sup> -Mont	161.62	37.132	7.5016	0.2965	0.3031

results of this investigation are illustrated in Table 2. As seen, performing the model reaction in various solvents and under reflux conditions led to poor yield of the final product. However, irradiation under microwaves (850 W) in solvent-free conditions dramatically accelerated the reaction rate to afford biscoumarin **4c**, 3,3'-(4-chlorophenylmethylene)-bis(4-hydroxy-2*H*-chromen-2-one), in 95 % yield within 5 min. It is notable that use of larger quantities of Ni<sup>0</sup>-Mont catalyst did not accelerate the rate of reaction. In addition, carrying out the model reaction with lower amounts of Ni<sup>0</sup>-Mont prolonged the reaction time. So, the conditions mentioned in entry 6 of Table 2 were selected as the optimum for complete conversion of 4-hydroxycoumarin (2 mmol) and 4-chlorobenzaldehyde to the corresponding biscoumarin **4c**.

The usefulness and catalytic activity of the Ni<sup>0</sup>-Mont system were also highlighted by comparing the synthesis of biscoumarin **4c** in the presence of Ni<sup>0</sup> nanoparticles alone as well as other modified montmorillonites under the optimized reaction conditions. The results of this investigation are illustrated in Table 3. This table shows that, among the examined catalyst systems, only the Ni<sup>0</sup>-Mont system efficiently catalyzed the reaction within 5 min affording the product in high yield. In this context, the Fe<sup>3+</sup>-Mont system could also be used for promotion of the title reaction. However, the transformation took a longer reaction time to give the product in slightly lower yield (Table 3, entry 5).

The scope and generality of this synthetic method were further studied by synthesis of structurally diverse biscoumarin compounds through microwave-assisted Knoevenagel condensation reaction of 4-hydroxycoumarin with substituted aromatic

**Table 2** Optimization experiments for synthesis of biscoumarin **4c** in presence of Ni<sup>0</sup>-Mont catalyst

Entry	Ni <sup>0</sup> -Mont (mg)	Solvent (2 mL)	Condition	Time (min)	Yield (%)
1	20	EtOH	Reflux	40	35
2	20	H <sub>2</sub> O	Reflux	120	30
3	20	EtOH–H <sub>2</sub> O (1:1)	Reflux	30	70
4	20	CH <sub>3</sub> CN	Reflux	120	20
5	10	Solvent-free	Microwave (850 W)	10	83
6	20	Solvent-free	Microwave (850 W)	5	95
7	30	Solvent-free	Microwave (850 W)	5	95
8	20	Solvent-free	Microwave (600 W)	20	80

aldehydes under solvent-free conditions. The results illustrated in Table 4 show the general trends and versatility of this synthetic protocol. As shown, all reactions were carried out within 5–15 min to afford the products in high to excellent yield.

The catalytic ability of the Ni<sup>0</sup>-Mont system in Knoevenagel reaction of 1,3-dicarbonyl compounds with aromatic aldehydes was further explored using the condensation reaction of 4-chlorobenzaldehyde (1 mmol) with dimedone (2 mmol) as model reaction. The results showed that the optimized reaction conditions for synthesis of biscoumarin **4c** were also efficient for synthesis of bisdimedone **5c**. Therefore, the reaction of arylaldehydes containing electron-withdrawing or electron-releasing functionalities with dimedone under solvent-free conditions with microwave irradiation (850 W) was investigated; The results are illustrated in Table 5, showing that all reactions were carried out successfully within 5–20 min to afford bisdimedones **5a–e** in high to excellent yield.

Although the exact mechanism of this synthetic method is not clear, the mechanism depicted in Scheme 3 could illustrate the role of Ni<sup>0</sup>-Mont clay in promoting the condensation reaction of 1,3-dicarbonyl compounds with aromatic aldehydes. The mechanism shows that, through polarization of formyl group with Ni<sup>0</sup>-Mont clay, formation of intermediate **I** is facilitated. Subsequently, by reaction of 1,3-dicarbonyl compound with intermediate **I**, intermediate **II** is produced. Finally, Michael addition of intermediate **II** with a second molecule of 1,3-dicarbonyl compound affords the final product **III**.

The usefulness and potentiality of the Ni<sup>0</sup>-Mont/microwave system for one-pot synthesis of biscoumarins are highlighted by comparison of the result obtained for biscoumarin **4c** with previously reported protocols to accomplish this transformation in Table 6. This survey reveals that, in terms of reaction time, reusability of the nanocatalyst, and yield of the desired products, the present work exhibits greater or comparable efficiency to previous systems.

## Recycling of Ni<sup>0</sup>-Mont catalyst

The green and economical features of the current protocol were further examined by studying the reusability of the Ni<sup>0</sup>-Mont catalyst in synthesis of biscoumarin

**Table 3** Microwave-assisted synthesis of biscoumarin **4c** catalyzed by Ni<sup>0</sup> NPs and other modified clay composite systems

Entry	Catalyst (20 mg)	Time (min)	Yield (%)
1	Ni <sup>0</sup> NPs	5	70
2	Mont K10	20	40
3	H <sup>+</sup> -Mont	15	60
4	Na <sup>+</sup> -Mont	20	40
5	Fe <sup>3+</sup> -Mont	10	85
6	Ni <sup>0</sup> -Mont	5	95
7	Mont-SO <sub>3</sub> H	10	70

All reactions carried out under microwave irradiation (850 W)

**Table 4** Microwave-assisted synthesis of biscoumarins in presence of Ni<sup>0</sup>-Mont system

Entry	Ar-	Product	Ni <sup>0</sup> -Mont (mg)	Time (min)	Yield (%) <sup>a</sup>	M.p. (°C)	
						Found	Reported
1	C <sub>6</sub> H <sub>4</sub>	<b>4a</b>	20	5	95	213–217	215–216 [76]
2	2,4-ClC <sub>6</sub> H <sub>3</sub>	<b>4b</b>	20	10	90	265–266	–
3	4-ClC <sub>6</sub> H <sub>4</sub>	<b>4c</b>	20	5	95	255–257	258–259 [47]
4	2-ClC <sub>6</sub> H <sub>4</sub>	<b>4d</b>	20	10	85	202–204	–
5	4-BrC <sub>6</sub> H <sub>4</sub>	<b>4e</b>	20	5	90	264–267	264–266 [47]
6	4-MeOC <sub>6</sub> H <sub>4</sub>	<b>4f</b>	20	5	90	247–249	249–250 [47]
7	2-MeOC <sub>6</sub> H <sub>4</sub>	<b>4g</b>	20	5	82	226–228	–
8	4-MeC <sub>6</sub> H <sub>4</sub>	<b>4h</b>	20	5	90	267–269	269–270 [77]
9	4-OHC <sub>6</sub> H <sub>4</sub>	<b>4i</b>	20	5	85	222–225	–
10	4-O <sub>2</sub> NC <sub>6</sub> H <sub>4</sub>	<b>4j</b>	20	5	90	232–234	238–239 [47]
11	2-O <sub>2</sub> NC <sub>6</sub> H <sub>4</sub>	<b>4k</b>	20	15	90	200–202	200–202 [76]
12	4-Pyridyl	<b>4l</b>	20	5	90	214–215	–

The condensation reactions were carried out with 1 mmol arylaldehyde and 2 mmol 4-hydroxycoumarin under microwave irradiation (850 W) under solvent-free conditions

<sup>a</sup>Yields refer to isolated pure products

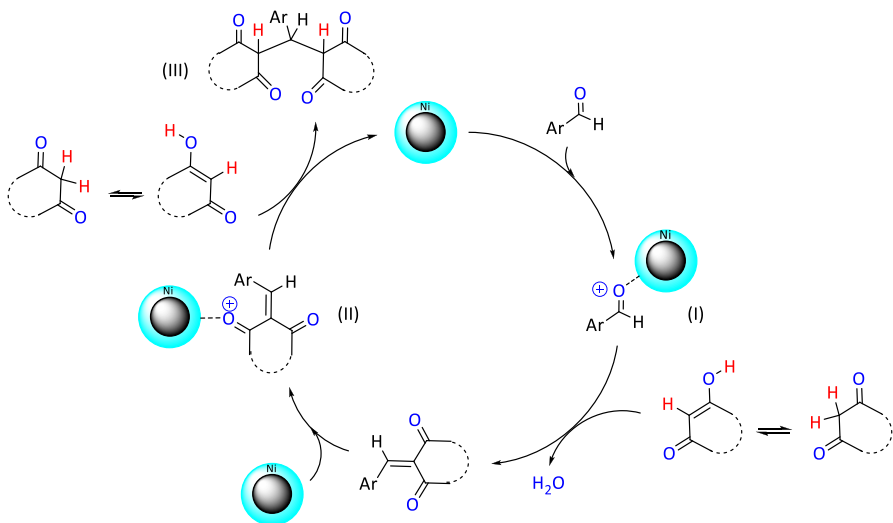
**4c.** After completion of the reaction, the catalyst was separated, washed with EtOH, then dried under air atmosphere. The reaction vessel was again charged with 4-chlorobenzaldehyde, 4-hydroxycoumarin, and the recycled Ni<sup>0</sup>-Mont clay to run the condensation reaction for a second time. The results shows that the clay catalyst could be reused in seven consecutive cycles without significant loss of catalytic activity (Fig. 7). In this context, XRD analysis showed that, through the recycling steps of Ni<sup>0</sup>-Mont catalyst, the clay matrix lost the anchored nickel content from interlamellar spaces (Fig. 8). It is clearly seen that the absorption signals for nickel species decreased after seven recycling steps.

**Table 5** Microwave-assisted synthesis of bisdimedones catalyzed by Ni<sup>0</sup>-Mont clay

Entry	Ar-	Product	Time (min)	Yield (%) <sup>a</sup>	M.p. (°C)
1	C <sub>6</sub> H <sub>4</sub>	<b>5a</b>	15	90	195–196
2	2-ClC <sub>6</sub> H <sub>4</sub>	<b>5b</b>	8	95	136–137
3	4-ClC <sub>6</sub> H <sub>4</sub>	<b>5c</b>	5	95	140–142
4	3-OH,4-MeOC <sub>6</sub> H <sub>3</sub>	<b>5d</b>	20	75	170–172
5	4-O <sub>2</sub> NC <sub>6</sub> H <sub>4</sub>	<b>5e</b>	10	95	196–197

The condensation reactions were carried out with 1 mmol aromatic aldehyde and 2 mmol dimedone under microwave irradiation (850 W) under solvent-free conditions

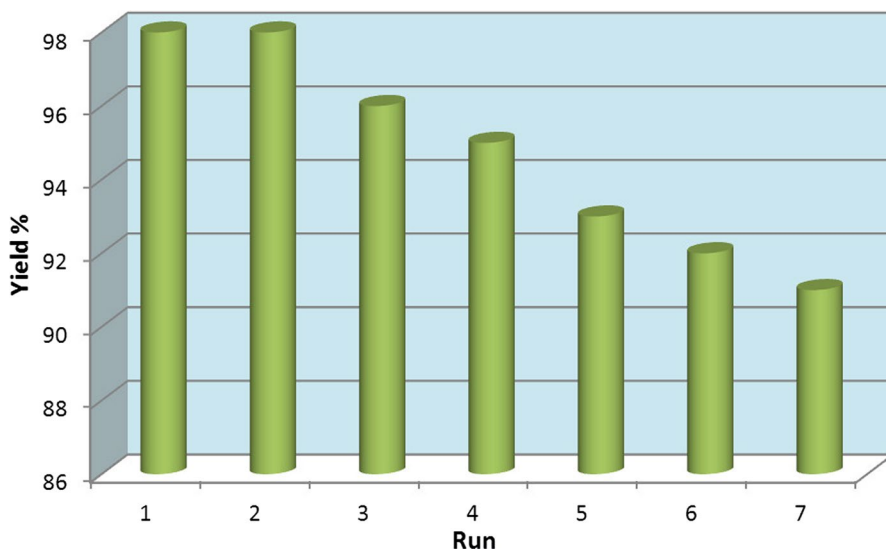
<sup>a</sup>Yields refer to isolated pure products



**Scheme 3** Proposed mechanism for Knoevenagel reaction of arylaldehydes with 1,3-dicarbonyl compounds catalyzed by Ni<sup>0</sup>-Mont clay

**Table 6** Comparison of one-pot synthesis of biscoumarin **4c** with Ni<sup>0</sup>-Mont and other reported catalysts

Entry	Catalyst	Time (min)	Yield (%)	Condition	Reusability	References
1	Ni <sup>0</sup> -Mont/microwave	5	95	Solvent-free	7	<sup>a</sup>
2	Polyvinyl pyrrolidone-Ni NPs	15	92	r.t.	4	[78]
3	Sulfated titania	15	96	80 °C	5	[79]
4	<i>n</i> -Dodecylbenzene sulfonic acid (DBSA)	60	87	40 °C	–	[80]
5	Silica-bonded <i>N</i> -propyl piperazine sodium <i>n</i> -propionate	15	92	Reflux	5	[81]
6	Sodium dodecyl sulfate (SDS)	150	95	60 °C	5	[51]
7	Boiling EtOH	750	44	Reflux	–	[82]
8	SO <sub>3</sub> H-functionalized ionic liquids	120	96	70 °C	2	[83]
9	TBAB	30	95	Reflux	–	[53]
10	Piperidine	240	95	r.t.	–	[48]

<sup>a</sup>Present work**Fig. 7** Reusability of Ni<sup>0</sup>-Mont system in synthesis of biscoumarin **4c**

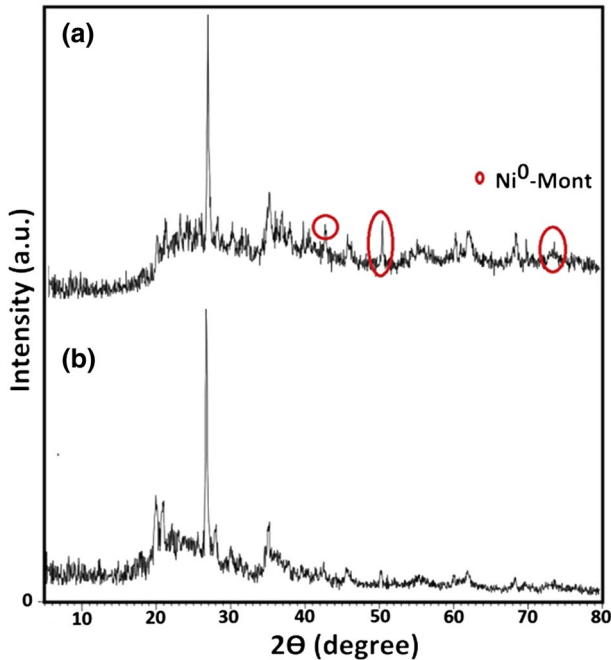


**Fig. 8** Wide-angle XRD pattern of Ni<sup>0</sup>-Mont catalyst **a** before recycling and **b** after seven recycling steps

## Conclusions

We investigated immobilization of Ni<sup>0</sup> NPs on acid-activated montmorillonite (Ni<sup>0</sup>-Mont). The prepared clay composite system was then characterized using FT-IR spectroscopy, SEM, EDX spectroscopy, XRD analysis, and BET analysis. The catalytic activity of the Ni<sup>0</sup>-Mont system was studied in microwave-assisted Knoevenagel condensation reaction of 4-hydroxycoumarin/dimedone with structurally diverse aromatic aldehydes under solvent-free conditions. All reactions were carried out in presence of 20 mg of the clay composite, affording the products in high to excellent yield. The examined Ni<sup>0</sup>-Mont system was recovered and reused in seven consecutive cycles without significant loss of catalytic activity. This protocol exhibits some advantages in terms of short reaction time, high product yield, and excellent reusability of the Ni<sup>0</sup>-Mont system, as well as the advantage of solvent-free conditions. It can thus be considered as a prominent choice for synthesis of biscoumarin and bisdimedone materials.

**Acknowledgements** The authors gratefully acknowledged financial support of this work by the research council of Urmia University.

## References

1. X. Xie, Y. Li, Z.Q. Liu, M. Haruta, W. Shen, *Nature* **458**, 746 (2009)
2. C.N. Ramachandra Rao, G.U. Kulkarni, P.J. Thomas, P.P. Edwards, *Chem. Soc. Rev.* **29**, 27 (2000)
3. E. Formo, E. Lee, D. Campbell, Y. Xia, *Nano Lett.* **8**, 668 (2008)
4. N. Zheng, G.D. Stucky, *J. Am. Chem. Soc.* **128**, 14278 (2006)
5. Z. Huang, F. Cui, H. Kang, J. Chen, X. Zhang, C. Xia, *Chem. Mater.* **20**, 5090 (2008)
6. B. Suresh Kumar, A. Dhakshinamoorthy, K. Pitchumani, *Catal. Sci. Technol.* **4**, 2378 (2014)
7. S. Bai, X. Shen, G. Zhu, M. Li, H. Xi, K. Chen, *ACS Appl. Mater. Interfaces* **4**, 2378 (2012)
8. F. Davar, Z. Fereshteh, M. Salavati-Niasari, *J. Alloys Compd.* **476**, 797 (2009)
9. L.K. Yeung, R.M. Crooks, *Nano Lett.* **1**, 14 (2001)
10. F.S. Han, *Chem. Soc. Rev.* **42**, 5270 (2013)
11. L. Wu, J. Ling, Z.Q. Wu, *Adv. Synth. Catal.* **353**, 1452 (2011)
12. Y.L. Zhao, Y. Li, S.M. Li, Y.G. Zhou, F.Y. Sun, L.X. Gao, F.S. Han, *Adv. Synth. Catal.* **353**, 1543 (2011)
13. F. Alonso, P. Riente, M. Yus, *Synlett* **9**, 1289 (2008)
14. S.Z. Tasker, A.C. Gutierrez, T.F. Jamison, *Angew. Chem. Int. Ed.* **53**, 1858 (2014)
15. W. Zhang, H. Qi, L. Li, X. Wang, J. Chen, K. Peng, Z. Wang, *Green Chem.* **11**, 1194 (2009)
16. C. Zheng, S.S. Stahl, *Chem. Commun.* **51**, 12771 (2015)
17. S.B. Sapkal, K.F. Shelke, B.B. Shingate, M.S. Shingare, *Tetrahedron Lett.* **50**, 1754 (2009)
18. J.M. Khurana, K.Vij Sneha, *Synth. Commun.* **42**, 2606 (2012)
19. M. Saha, B. Das, A. Kumar Pal, C. R. Chim. **16**, 1079 (2013)
20. T. Tsukatani, H. Fujihara, *Langmuir* **21**, 12093 (2005)
21. D. Dutta, B.J. Borah, L. Saikia, M.G. Pathak, P. Sengupta, D.K. Dutta, *Appl. Clay Sci.* **53**, 650 (2011)
22. J.D. Aiken, R.G. Finke, *J. Am. Chem. Soc.* **121**, 8803 (1999)
23. M. Tamura, H. Fujihara, *J. Am. Chem. Soc.* **125**, 15742 (2003)
24. V.K. Sharma, R.A. Yngard, Y. Lin, *Adv. Colloid Interface Sci.* **145**, 83 (2009)
25. N. Mahata, A.F. Cunha, J.J.M. Orfao, J.L. Figueiredo, *Appl. Catal.* **351**, 204 (2008)
26. F. Schröder, D. Esken, M. Cokoja, M.W. van den Berg, O.I. Lebedev, G. Van Tendeloo, B. Walaszek, G. Buntkowsky, H.H. Limbach, B. Chaudret, R.A. Fischer, *J. Am. Chem. Soc.* **130**, 6119 (2008)
27. D.H. Chen, C.H. Hsieh, *J. Mater. Chem.* **12**, 2412 (2002)
28. J.M. Campelo, T.D. Conesa, M.J. Gracia, M.J. Jurado, R. Luque, J.M. Marinas, A.A. Romero, *Green Chem.* **10**, 853 (2008)
29. S. Pande, A. Saha, S. Jana, S. Sarkar, M. Basu, M. Pradhan, A.K. Sinha, S. Saha, A. Pal, T. Pal, *Org. Lett.* **10**, 5179 (2008)
30. M.L. Kantam, R. Chakravarti, U. Pal, B. Sreedhar, S. Bhargava, *Synfacts* **7**, 767 (2008)
31. Z. Király, I. Dékány, Á. Mastalir, M. Bartók, *J. Catal.* **161**, 401 (1996)
32. P. Sharma, S.K. Bhorodwaj, D.K. Dutta, in *Journal of Scientific Conference Proceedings* (American Scientific Publishers, 2009), p. 40
33. A. Gil, S.A. Korili, R. Trujillano, M.A. Vicente, *Pillared Clays and Related Catalysts* (Springer, Heidelberg, 2010)
34. O.S. Ahmed, D.K. Dutta, *Langmuir* **19**, 5540 (2003)
35. P.B. Malla, P. Ravindranathan, S. Komarneni, R. Roy, *Nature* **351**, 555 (1991)
36. R.S. Varma, *Tetrahedron* **58**, 1235 (2002)
37. I. Manolov, C. Maichle-Moessner, N. Danchev, *Eur. J. Med. Chem.* **41**, 882 (2006)
38. E. Adami, U.E. Marazzi, C. Turba, *Arch. Ital. Sci. Farmacol.* **9**, 61 (1959)
39. Z.H. Chohan, A.U. Shaikh, A. Rauf, C.T. Supuran, *J. Enzyme Inhib. Med. Chem.* **21**, 741 (2006)
40. N. Hamdi, M.C. Puerta, P. Valerga, *Eur. J. Med. Chem.* **43**, 2541 (2008)
41. A.C. Luchini, P. Rodrigues-Orsi, S.H. Cestari, L.N. Seito, A. Witaicenis, C.H. Pellizzon, L.C. Di Stasi, *Biol. Pharm. Bull.* **31**, 1343 (2008)
42. D.H. Mahajan, C. Pannecouque, E. De Clercq, K.H. Chikhaliya, *Arch. Pharm. (Weinheim)* **342**, 281 (2009)
43. M.A. Velasco-Velázquez, J. Agramonte-Hevia, D. Barrera, A. Jiménez-Orozco, M.A.J. García-Mondragón, N. Mendoza-Patiño, A. Landa, J. Mandoki, *Cancer Lett.* **198**, 179 (2003)

44. D. Završnik, S. Muratović, D. Makuc, J. Plavec, M. Cetina, A. Nagl, E.D. Clercq, J. Balzarini, M. Mintas, *Molecules* **16**, 6023 (2011)
45. M. Gersch, J. Kreuzer, S.A. Sieber, *Nat. Prod. Rep.* **29**, 659 (2012)
46. K. Petnapapun, W. Chavasiri, P. Sompornpisut, *Sci. World J.* **2013**, 178649 (2013)
47. M. Kidwai, V. Bansal, P. Mothra, S. Saxena, R.K. Somvanshi, S. Dey, T.P. Singh, *J. Mol. Catal. A Chem.* **268**, 76 (2007)
48. K.H. Khan, S. Iqbal, M.A. Lodhi, G.M. Maharvi, Z. Ullah, M.I. Choudhary, A.U. Rahman, S. Perveen, *Bioorgan. Med. Chem.* **12**, 1963 (2004)
49. H. Hagiwara, N. Fujimoto, T. Suzuki, M. Ando, *Heterocycles* **53**, 549 (2000)
50. A. Shamsaddini, E. Sheikhhosseini, *Int. J. Org. Chem.* **4**, 135 (2014)
51. H. Mehrabi, H. Abusaidi, *J. Iran. Chem. Soc.* **7**, 890 (2010)
52. Z.N. Siddiqui, T.N. Mohammed Musthafa, S. Praveen, F. Farooq, *Med. Chem. Res.* **20**, 1438 (2011)
53. J.M. Khurana, S. Kumar, *Tetrahedron Lett.* **50**, 4125 (2009)
54. A. Tzani, A. Douka, A. Papadopoulos, E.A. Pavlatou, E. Voutsas, A. Detsi, *ACS Sustain. Chem. Eng.* **1**, 1180 (2013)
55. R. Karimian, F. Piri, A.A. Safari, S.J. Davarpanah, *J. Nanostruct. Chem.* **3**, 52 (2013)
56. A.M. Al-Majid, M. Shahidul Islam, A. Barakat, N.J. Al-Qahtani, S. Yousuf, M. Iqbal Choudhary, *Arab. J. Chem.* **10**, 185 (2017)
57. D. Arora, J. Dwivedi, S. Kumar, D. Kishore, *Synth. Commun.* **48**, 115 (2018)
58. A.G. Banerjee, L.P. Kothapalli, P.A. Sharma, A.B. Thomas, R.K. Nanda, S.K. Shrivastava, V.V. Khatanglekar, *Arab. J. Chem.* **9**, S480 (2016)
59. S.A. Hilderbrand, R. Weissleder, *Tetrahedron Lett.* **48**, 4383 (2007)
60. G. Pohlers, J. Scaliano, R. Sinta, *Chem. Mater.* **9**, 3222 (1997)
61. C.G. Knight, T. Stephens, *Biochem. J.* **258**, 683 (1989)
62. S. Hatakeyama, N. Ochi, H. Numata, S. Takano, *J. Chem. Soc. Chem. Commun.* **17**, 1202 (1988)
63. M.A. Mekewi, A.S. Darwish, M.S. Amin, G. Eshaq, H.A. Bourazan, *Egypt. J. Petrol.* **25**, 269 (2016)
64. R. Das, S.S. Nath, R. Bhattacharjee, *J. Fluoresc.* **21**, 1165 (2011)
65. B. Bagchi, S. Kar, S.K. Dey, S. Bhandary, D. Roy, T.K. Mukhopadhyay, S. Das, P. Nandy, *Colloid Surf. B Biointerfaces* **108**, 358 (2013)
66. B. Sahin, T. Kaya, *Appl. Surf. Sci.* **362**, 532 (2016)
67. E. Şennik, S. Kerli, Ü. Alver, Z.Z. Öztürk, *Sens. Actuators B* **216**, 49 (2015)
68. S.K. Bhorodwaj, D.K. Dutta, *Appl. Catal. A* **378**, 221 (2010)
69. L. Saikia, D. Dutta, D.K. Dutta, *Catal. Commun.* **19**, 1 (2012)
70. A. Dhakshinamoorthy, K. Pitchumani, *Tetrahedron Lett.* **49**, 1818 (2008)
71. S. Brunauer, L.S. Deming, W.E. Deming, E. Teller, *J. Am. Chem. Soc.* **62**, 1723 (1940)
72. G.B.B. Varadwaj, S. Rana, K. Parida, *Chem. Eng. J.* **215–216**, 849 (2013)
73. P.K. Saikia, P.P. Sarmah, B.J. Borah, L. Saikia, K. Saikia, D. Kumar Dutta, *Green Chem.* **18**, 2843 (2016)
74. J. Ji, P. Zeng, S. Ji, W. Yang, H. Liu, Y. Li, *Catal. Today* **158**, 305 (2010)
75. S.K. Bhorodwaj, M.G. Pathak, D.K. Dutta, *Catal. Lett.* **133**, 185 (2009)
76. S. Qadir, A. Ahmad Dar, K. Zaman Khan, *Synth. Commun.* **38**, 3490 (2008)
77. N. Tavakoli-Hoseini, M.M. Heravi, F.F. Bamoharram, A. Davoodnia, M. Ghassemzadeh, *J. Mol. Liq.* **163**, 122 (2011)
78. J.M. Khurana, K. Vij, *J. Chem. Sci.* **124**, 907 (2012)
79. B. Karmakar, A. Nayak, J. Banerji, *Tetrahedron Lett.* **53**, 4343 (2012)
80. B. Pawar, V. Shinde, A. Chaskar, *Green Sustain. Chem.* **3**, 56 (2013)
81. K. Niknam, A. Jamali, *Chin. J. Catal.* **33**, 1840 (2012)
82. I. Manolov, C. Maichle-Moessner, I. Nicolova, N. Danchev, *Arch. Pharm.* **339**, 319 (2006)
83. W. Li, Y. Wang, Z. Wang, L. Dai, Y. Wang, *Catal. Lett.* **141**, 1651 (2011)